J. Cent. South Univ. (2014) 21: 2857−2865
DOI: 10.1007/s11771-014-2251-6

Springer

Mechanical genesis of Henan (China) Yima thrust nappe structure

CAI Wu(蔡武)[1], DOU Lin-ming(窦林名)[1], HE Jiang(何江)[1],
LIU Hai-shun(刘海顺)[2], LI Zhen-lei(李振雷)[1], DING Yan-lu(丁言露)[1]

1. State Key Laboratory of Coal Resources and Safe Mining
(China University of Mining and Technology), Xuzhou 221116, China;
2. School of Sciences, China University of Mining and Technology, Xuzhou 221116, China

Abstract: Considering the serious coal and rock dynamic disasters around the main slip plane called F16 in the coal mining area) of Henan Yima (China) thrust nappe structure, the mechanical genesis of the Yima thrust nappe structure was studied comprehensively using geomechanics, fault mechanics, elastic mechanics, and Coulomb's law of friction. First, using the centrifugal inertia force of Earth's rotation as a source, a mechanical model of N-S compression superimposed with W-E reverse torsion was established to explain the formation of the early Yima coal basin and Jurassic Yima Group coal measures. Second, an equation for the ultimate stress in the forming stage of F16 was derived using the plastic slip-line field theory and the parabolic Mohr failure criterion. Moreover, the distribution of ultimate stress and the geometric characteristics of the fault profile were obtained using the field model parameters. Finally, the stress field of F16 and the mechanical genesis of the large-scale reverse thrust sheet were discussed based on elastic mechanics theory and Coulomb's law of friction. The results show that the tectonic framework of the early Yima coal basin and the formation pattern of Jurassic Yima Group coal measures given by the model are consistent with the in-situ explorations. The geometric characteristics of the fault profile obtained by numerical calculation can better reflect the shape of F16 in its forming stage, and the mechanical genesis of the large-scale reverse thrust sheet also concurred with the field situations. Thus, this work can provide a foundation for further studies on the genesis of the thrust nappe structure, the mechanism of rock bursts induced by F16, and the characteristics of the residual stress field in the Yima mining area.

Key words: mechanical genesis; thrust nappe structure; centrifugal inertia force; fault mechanics; slip-line field theory; Coulomb's law of friction

1 Introduction

Studies show that disasters involving underground engineering, including mining, underground plants, water conservancy and hydropower, tunnels, and national defence, are closely related to faulted structures. When underground projects are located near faulted structures, disasters such as rock bursts, collapsed chambers, and inrushes of water become more frequent [1−2]. Research on the genesis of faulted structures can help us understand stress distributions to prevent engineering disasters underground.

The main slip plane (called F16 in the coal mining area) of the Henan Yima thrust nappe structure is a regional compression-shear fault across the Changcun, Yuejin, Qianqiu, Gengcun and Yangcun coal mines. The structure extends 24 km along the coalfield and constitutes its southern natural boundary (Fig. 1). As the depth of the main mine in the Yima mining area increased, the operation space gradually approached F16, resulting in a strong stress concentration. As for coal-rock dynamic disasters, such as rock bursts, roof cavings, rib spallings, and mining tremors, have increased sharply, especially in the Yuejin, Changcun and Qianqiu coal mines. For example, a rock burst accident (equivalent to M_w4.1) caused 10 deaths and trapped 75 people at 7:18 pm on November, 3, 2011 at the Qianqiu 21221 driving face. Therefore, it is essential to ascertain the background stress field of the Yima thrust nappe structure and its mechanical genesis.

The Yima thrust nappe structure has been studied extensively. CAO et al [3−4] claimed that the evolution of the Yima coal basin could be divided into three stages from the point of coal accumulation: early basin formation, basin expansion, and basin systolic. In

Foundation item: Project(2010CB226805) supported by the National Basic Research Program of China; Project(CXLX13-949) supported by the Research and Innovation Project for College Graduates of Jiangsu Province, China; Project(51174285) supported by the National Natural Science Foundation of China; Project(SZBF2011-6-B35) supported by the Priority Academic Program Development of Jiangsu Higher Education Institutions, China
Received date: 2013−03−06; **Accepted date:** 2013−10−01
Corresponding author: DOU Lin-ming, Professor, PhD; Tel: +86−516−83995904; E-mail: lmdou@cumt.edu.cn

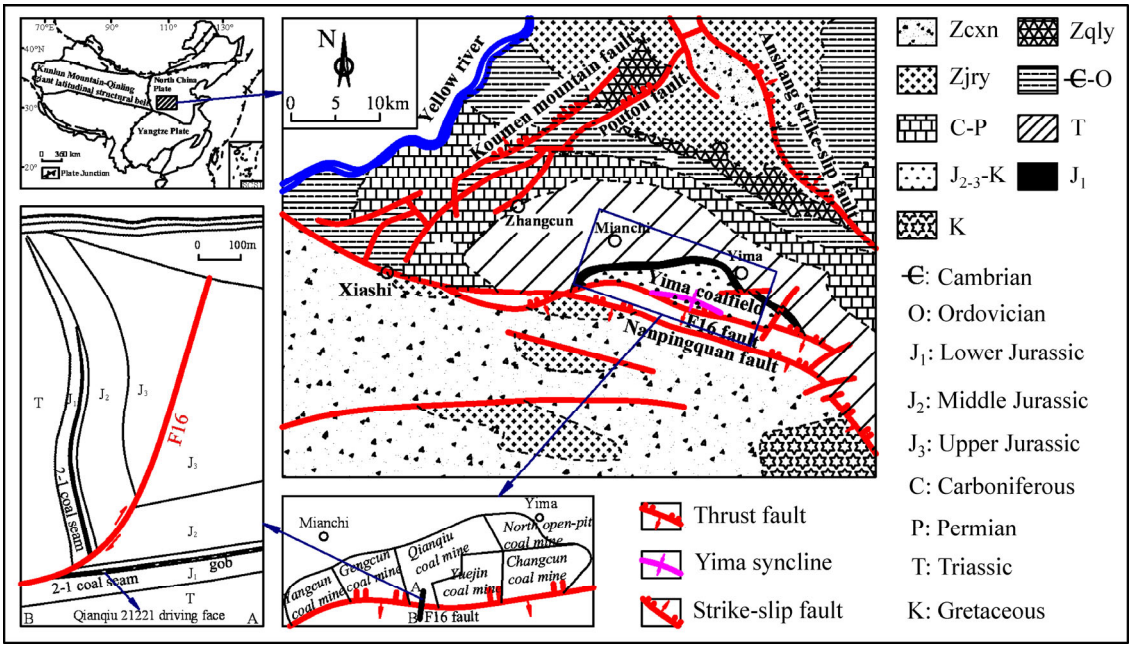

Fig. 1 Geological sketch map of Yima coal basin (Zcxn, Zjry, and Zqly indicate Xiong'er Group (early Paleozoic, Pt-1), Ruyang group (Mesoproterozoic, Pt-2), and Luoyu group (Neoproterozoic, Pt-3), respectively. SCSI is the abbreviation for South China Sea Islands)

addition, the basic characteristics and the mechanical genesis of the thrust nappe tectonic zone along the southern margin of North China's coal accumulation region were described from the perspective of its large tectonic background. CHEN et al [5−6] divided the development history of the Yima coal basin structure into an early expansion sinking stage and advanced compression upswing from the point of the basin-fill features, sedimentary environments, and ancient flow evolution. Moreover, the geometry, kinematics, and dynamics of the Yima thrust nappe structure were also elaborated. Former studies outlined the Yima thrust nappe structure; however, most focused qualitatively on engineering records, and few concerned themselves quantitatively with the mechanical genesis and formation processes.

Theoretical research regarding the study of fault mechanics can be divided into three stages: 1) stress state analysis; 2) stress field analysis; 3) slip-line field theory, which is a comprehensive application of balance equations and failure criteria [7−8]. NYE [9] first adopted the slip-line field theory to analyse the flow of glaciers, which was successfully applied in numerous applications [10−15]. CHEN [13] provided a reasonable explanation for the occurrence and patterns of listric faults and the mechanical properties of their gravitational structure based on the slip-line field theory for plastic plane strain obeying the parabolic Mohr failure criterion. MA et al [16] qualitatively explicated the mechanism for the development of a thrust fault and proposed the new viewpoint that the rupture of a thrust fault develops upward using a mechanical model that combines material mechanics and fracture mechanics. DI DOMENICA et al [17] provided a new insight to describe the relationships between thrusts and normal faults in curved belts. Recently, a new theory of maximum effective moment criterion proposed by ZHENG et al [18−19] has been a research highlight. It can reasonably interpret low-angle normal faults, high-angle thrust faults and many structures in anisotropic or plastic mediums. Moreover, LISLE and WAIKER [20] adopted the separation-pitch diagram to estimate fault slip, which was considered as a useful device for the representation of the kinematic characteristics of a collection of faults.

The aim of this work is to discuss the mechanical genesis of the Henan Yima thrust nappe structure from the point of the evolution of the Yima coal basin. The primary research focuses on the formation of the early Yima coal basin and Jurassic Yima Group coal measures, the formation and stress field of F16, and the mechanism genesis of the large-scale reverse thrust sheet.

2 Regional geology and structural features

The Yima Jurassic coal basin is a closed intermountain faulted basin that developed on the top of the triangular Mianchi faulted block, which is surrounded by the Anshang strike-slip fault in the northeast, the Koumen mountain-Potou fault in the northwest and the EW-trending Nanpingquan fault in the south. From north to south, the sequential outcrops are Proterozoic and Cambrian-Ordovician, Carboniferous,

Permian, Triassic, Jurassic, and Cretaceous. They generally constitute an incomplete syncline (Fig. 1).

The Yima thrust nappe structure is located on the north side of the EW Qinling tectonic zone. Its formation and late deformation are dominated by the tectonic activity of the EW tectonic zone since the Mesozoic. It is worth noting that the Qinling tectonic zone, which belongs to the Kunlun Mountain-Qinling giant latitudinal structural belt (Fig. 1), is a regional EW tectonic zone. F16 extends approximately 45 km along the strike (110°, dip to the south from east), 50−500 m in the fault throw and 120−1080 m in the horizontal offset. The geometric characteristic of the profile is a listric type with up-steep and down-gentle. The rigid conglomerate of the Upper Middle Jurassic is sheared by the shallow part of F16 with a dip angle of 75°. The deep part is 15°−35°. The succession in the footwall is involved in a syncline with an approximately EW-trending axial trend and the strata in the hanging wall are approximately sub-vertical, thrusting up northward along the Yima Group coal layer (Fig. 1).

Former research indicated that the Yima coal basin initiated during the Late Triassic and terminated in the Late Cretaceous [6]. The collision suture between the Yangtze and North China paleo-continent plates, due to the Indosinian movement of the Late Triassic, laid the framework for the Yima faulted basin, providing a place for coal accumulation for the Early Jurassic. Subsequent tectonics during the period of the Yanshan movement determined the development and propagation of the Yima faulted basin, including the development of a large-scale thrust nappe structural system. Ultimately, the large-scale nappe formed, and its stress has been released since the Late Cretaceous, accompanied by the end of the sedimentary history of the Yima coal basin. Its evolution is shown in Fig. 2 [6].

3 Driving force

Some researches indicated that there was a kind of close relationship between variable Earth's rotation rate and some geophysical phenomena, such as the tectonic framework of the Earth [21−22], earthquakes [23], ENSO events [24], crustal deformation [25−26], and atmospheric tides [27]. Thus, astronomers, geophysicist and experts on disasters pay attention to the research of variable Earth's rotation rate and geophysical phenomena.

LI [21] first proposed the hypothesis of continental brakes in the early twenties. He stated that the cyclical variations in the speed of the Earth's rotation during its long geological history were the main reason for seawater movement and rock deformation. His fundamental idea is that the centrifugal force varies with the angular velocity of the Earth's rotation, and the substances of the Earth's surface are driven by the horizontal component of the centrifugal force in longitudinal and latitudinal directions for balanced and unbalanced horizontal movements.

3.1 Centrifugal inertia force of Earth's rotation

With the Earth's rotation, the centrifugal inertia forces of longitude F and latitude f_s are generated at any point A on the Earth's spherical surface, as shown in Fig. 3 and Eq. (1):

$$\begin{cases} F = m\omega^2 R\cos\alpha \\ f_s = m\dfrac{\mathrm{d}\omega}{\mathrm{d}t}R\cos\alpha \end{cases} \tag{1}$$

where m is the mass of the particle A, ω is the angular velocity of the Earth's rotation, R is the distance between particle A and the Earth's core, and α is the geocentric latitude.

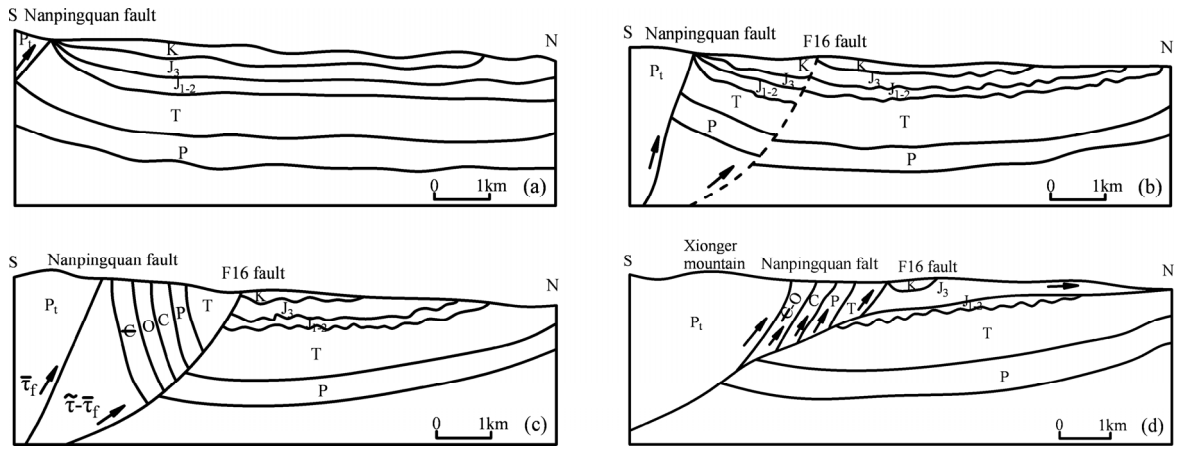

Fig. 2 Evolution diagram of Yima thrust nappe structure: (a) Sedimentary state of Yima coal basin; (b) F16 fault forming with Nanpingquan fault becoming active; (c) Strata in south of F16 thrust northward with Nanpingquan fault being strongly active; (d) All levels of slip planes formed, and overall development of thrust nappe structure completed

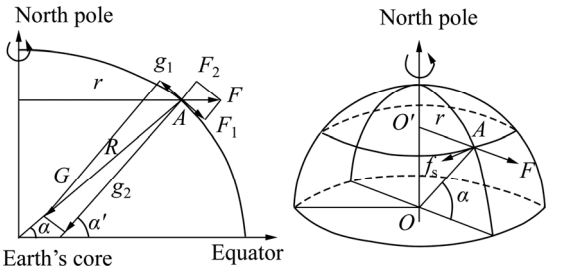

Fig. 3 Schematic diagram of centrifugal inertia forces generated by Earth's rotation

If the angular velocity produces an incremental change $\Delta\omega$, the incremental changes for the centrifugal inertia forces longitudinally are

$$\begin{cases}\Delta F_1 = 2m\dfrac{\Delta\omega}{\omega}\omega^2 R\cos\alpha\sin\alpha' \\ \Delta F_2 = 2m\dfrac{\Delta\omega}{\omega}\omega^2 R\cos\alpha\cos\alpha'\end{cases} \tag{2}$$

where α' is the geographic latitude, which is nearly equal to α.

Hereinto, ΔF_2 counterbalances some vertical component of gravity and ΔF_1 is the driving force for generating the latitudinal structural system for the Earth's crust. When the angular velocity of the Earth's rotation increases, $\Delta\omega$ is positive and ΔF_1 points to the equator. If $\Delta\omega$ is negative, ΔF_1 points to the South or North Pole. In other words, flattening of the Earth increases when the Earth's rotation accelerates, and the substance of upper crust tends to be driven from high latitudes to the equator, and vice versa. Equation (2) demonstrates that if $\cos\alpha=0$, $\Delta F_1=0$ on the poles; by contrast, if $\sin\alpha'\approx0$, $\Delta F_1\approx0$ at the equator. ΔF_1 is maximal when $\alpha=45°$ and $\cos\alpha\sin\alpha'\approx0.5$ in the middle latitudes.

Similarly, if $\mathrm{d}\omega/\mathrm{d}t\geq0$, then f_s occurs from east to west as the Earth's rotation speeds up. By contrast, f_s occurs from west to east. $f_s=0$ on the poles, and f_s is maximal and its direction is parallel to latitudinal lines at the equator.

3.2 Evidence of variation of angular velocity of Earth's rotation

Since the Palaeozoic, the speed of the Earth's rotation has decreased and the radius of the Earth has increased [28]: OWEN [29] proposed that the radius of the Earth in the Jurassic was 80% of its present size; GLIKSON [30] approximated that it was 60% in the Precambrian; WANG [31] approximated the radius to be 75%, 80%, 85%, 90% and 95% of its present size in P-2500 Ma, P-1950 Ma, P-1450 Ma, P-850 Ma and P-250 Ma, respectively. According to the angular momentum conservation, $mr^2\omega=c$ (c is constant, $r=R\cos\alpha$), the speed of the Earth's rotation and the number of days per year decrease as the radius of the Earth increases.

WELLS [32] showed that there were 424 days in the Cambrian, 402 days in the Silurian, 385 days in the Permian, and 377 days in the Jurassic, eventually decreasing to 365 days in a year today. And the change of the average days in a lunar month was summarised [33] since the Palaeozoic (Fig. 4).

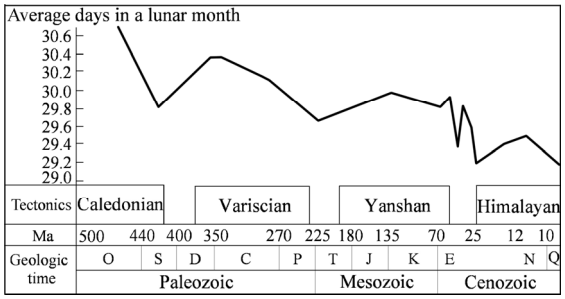

Fig. 4 Relation between average days in a lunar month and geological time since the Paleozoic

The following rules can be concluded: 1) the angular velocity of the Earth has generally decreased since the Palaeozoic; 2) the speed of the Earth's rotation is sometimes quick and sometimes slow, representing a certain periodicity; 3) since the Palaeozoic, the Earth's speed has experienced four major turning points: 440 Ma (from deceleration to acceleration), 350 Ma (from acceleration to deceleration), 230 Ma (from deceleration to acceleration) and 130 Ma (from acceleration to deceleration).

4 Mechanical geneses of early Yima basin and Yima Group coal measures

The in-site data of the Yima basin indicate that the sedimentary basin of the Carboniferous and Triassic in North China disintegrated due to the Indosinian Late Triassic movement, resulting in the formation of the Yima basin. From the perspective of the greater region, the focus of this work is located between the middle latitudes and low latitudes of the northern hemisphere, represented approximately as rectangular block ABCD (Fig. 5). During the Indosinian movement, the angular velocity of the Earth's rotation increased and the lithospheric plate moved toward the equator, generating a squeezing action from the equator to the poles; thus, block ABCD had been subjected to extrusion in the N-S direction (Fig. 5). In addition, due to the northern boundary of the ABCD being located in the middle latitudes, the effective radius of rotation for a particle on the northern boundary was maximally small and its rotation rate was significantly faster than a particle on the southern boundary, which was located in the low latitudes. f_s was also greater based on Eq. (1). Therefore, the force of the W-E reverse torsion was

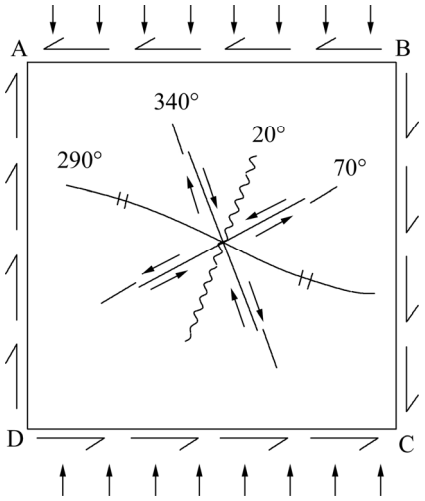

Fig. 5 Mechanical model of N-S compression superimposed with W-E reverse torsion and a sketch map of its structural style

generated as f_s occurred from east to west (Fig. 5).

According to the mechanical model (Fig. 5), with the orientation of the maximum principal stress in a NNE-SSW direction, the extrusion uplifted belt with an axial direction in the NWW and the thrust fault with a strike in the NWW could have formed. In addition, the normal fault, the strike-slip fault of anticlockwise torsion and the strike-slip fault of clockwise torsion, which strike NNE, NEE and NNW, respectively, could have formed because of the conversion of a minimum principal stress axis and an intermediate principal stress axis during the process of deformation.

Hence, the tectonic framework of the early Yima triangle faulted coal accumulation basin, which strikes approximately NWW, could be expounded by a mechanical model with N-S compression superimposed with W-E reverse torsion, which explained the Nanpingquan thrust fault; the Koumen Mountain-Potou fault, which strikes NNE; and the Anshang strike-slip fault, which strikes NNW.

Furthermore, with speed of the Earth's rotation increasing during the Jurassic, a squeezing action from the poles to the equator was generated. The violent movement of the Koumen Mountain-Potou fault and the Anshang strike-slip fault and the relatively weak movement of the Nanpingquan fault resulted in uplifting in the north and depressing in the south of the Yima coal basin. During this period, the basin mainly collected the terrigenous clastic substances originating from the north side, and the Jurassic Yima Group coal measures were finally formed (Fig. 2(a)).

5 Mechanical genesis of F16 thrust fault

In the Late Jurassic, speed of the Earth's rotation began to decrease and the lithospheric plate began to move from the equator to the poles, leading to the strong movement of the Nanpingquan fault. The strata of the Proterozoic and the Palaeoproterozois in the south of the fault were uplifted in a large area, accompanied with large-scale magmatism. Gravity spreading occurred in the uplifted edge zone, resulting in large-scale compressive stress. Afterwards, the Yima thrust nappe structure began to initiate, especially the F16 thrust fault, which was the first to be initiated and propagated.

5.1 Mechanical model and failure criterion of rocks

According to the mechanical model of the gravitational gliding layer [9,13], as shown in Fig. 6, the analytical expression can be expressed by effective stress as follows:

$$\begin{cases}\widetilde{\tau}_{zx}=\gamma z\sin\theta\\ \widetilde{\sigma}_{z}=\gamma z\cos\theta(1-\lambda)\end{cases} \tag{3}$$

where θ is the gradient of the sliding system; γ is the stress gradient of fluid-filled rocks; $\widetilde{\tau}_{zx}$ and $\widetilde{\sigma}_{z}$ are effective stresses; λ is the ratio of the pore fluid pressure to the geostatic stress.

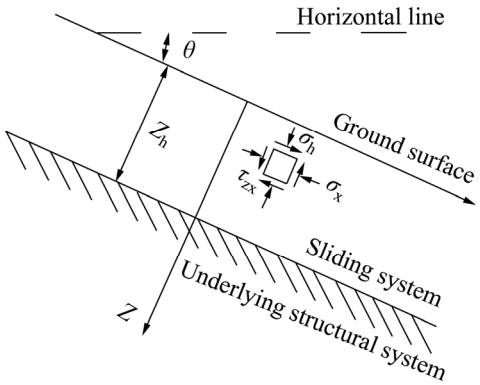

Fig. 6 Mechanical model of gravitational gliding layer

Herein, the parabolic Mohr failure criterion [34] was employed:

$$\tau^2=n(\sigma+\sigma_{\mathrm{t}}) \tag{4}$$

where σ_{t} is the uniaxial tensile strength; $n=c^2/\sigma_{\mathrm{t}}$, is the undetermined coefficient; c is the cohesion.

An expression for the parabolic Mohr envelope using stress components in axes can be deduced as

$$(\widetilde{\sigma}_x-\widetilde{\sigma}_z)^2=2n(\widetilde{\sigma}_x+\widetilde{\sigma}_z)+4n\sigma_{\mathrm{t}}-n^2-4\widetilde{\tau}_{zx}^2 \tag{5}$$

5.2 Distribution of ultimate stress and fracture plane of system

For rocks obeying the parabolic Mohr failure criterion, expressed in terms of effective stress (Eq. (5)), reaching the state of limit equilibrium means that each point in the sliding system satisfies the criterion. Thus,

the limit stress states can be given by substituting Eq. (3) into Eq. (5):

$$\begin{cases}\widetilde{\sigma}_z=\gamma z\cos\theta(1-\lambda)\\ \widetilde{\tau}_{zx}=\gamma z\sin\theta\\ \widetilde{\sigma}_x=(\widetilde{\sigma}_z+n)\pm 2\sqrt{n(\sigma_t+\widetilde{\sigma}_z)-\widetilde{\tau}_{zx}^2}\end{cases} \tag{6}$$

Equation (6) shows that the sliding system can reach the state of ultimate stress only if $n(\sigma_t+\widetilde{\sigma}_z)-\widetilde{\tau}_{zx}^2\geq 0$. When $n(\sigma_t+\widetilde{\sigma}_z)-\widetilde{\tau}_{zx}^2=0$, the mass of the sliding system reaches critical equilibrium at $z=z_h$. Substituting $n(\sigma_t+\widetilde{\sigma}_z)-\widetilde{\tau}_{zx}^2=0$ and $z=z_h$ into Eq. (6) yields the following:

$$\begin{cases}\widetilde{\tau}_{zx}=\gamma z_h\sin\theta\\ \widetilde{\sigma}_z=\gamma z_h\cos\theta(1-\lambda)\\ z_h=\dfrac{n\gamma\cos\theta(1-\lambda)+\sqrt{n^2\gamma^2\cos^2\theta(1-\lambda)^2+4\gamma^2\sin^2\theta\sigma_t n}}{2\gamma^2\sin^2\theta}\\ \cos\theta=\dfrac{-n(1-\lambda)+\sqrt{n^2(1-\lambda)^2+4(\gamma^2z_h^2-\sigma_t n)}}{2\gamma z_h}\end{cases} \tag{7}$$

It is worth noting that the strengths (σ_t, n) in Eq. (7) are the strengths of the lubricating layer itself when the lubricating layer exists.

There are two solutions for $\widetilde{\sigma}_x$ ($\widetilde{\sigma}_x^+$ and $\widetilde{\sigma}_x^-$) in Eq. (6); thus, there are two states of ultimate stress: $\widetilde{\sigma}_x^+=(\widetilde{\sigma}_z+n)+2\sqrt{n(\sigma_t+\widetilde{\sigma}_z)-\widetilde{\tau}_{zx}^2}$, and $\widetilde{\sigma}_x^-=(\widetilde{\sigma}_z+n)-2\sqrt{n(\sigma_t+\widetilde{\sigma}_z)-\widetilde{\tau}_{zx}^2}$. Since the Yima thrust nappe structure thrusts up from south to north along the Yima Group coal seam, we took the coal seam as the low-strength layer. In order to properly design our models, we characterized the coal mechanical parameters using uniaxial compression and shear tests on in-situ samples derived from Yuejin, Changcun, Qianqiu and Gengcun coal mines. Results show that the uniaxial compression strength ranges from 10.1 to 20.4 MPa (16 MPa in average) and the cohesion c ranges from 1.14 to 3.12 MPa (2 MPa in average). Further, considering the anomalous pore pressure, the necessary parameters are as follows:

σ_t=1.6 MPa, c=2 MPa, γ=0.025 MPa/m, θ=5°, λ=0.9

Substituting the above parameters into Eqs. (4) and (7) yields

n=2.5 MPa, z_h=1783.78 m (8)

As a result, the relation between ultimate stress and depth can be obtained, as shown in Fig. 7.

It is known that $\widetilde{\sigma}_x^-$ changes from tensile stress to tensile shear, pure shear and compressive shear from top to bottom, called the extending deformation state, and $\widetilde{\sigma}_x^+$ is entirely compressive shear, called the compressive deformation state.

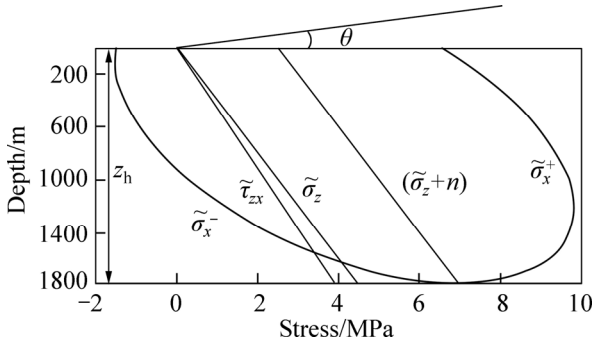

Fig. 7 Relation between ultimate stress and depth

The direction of the bedding is x-axis regarding the mechanical model of gravitational gliding layer (Fig. 6). Thus, the angle (β) between σ_1 and the x-axis under the limit equilibrium state is

$$\beta=0.5\arctan\left(\frac{2\widetilde{\tau}_{zx}}{\widetilde{\sigma}_x-\widetilde{\sigma}_z}\right) \tag{9}$$

According to the slip-line field theory, the slip-line can be obtained by connecting the lines of the direction of each point's fracture plane (also called slipping plane) when the materials are in a plastic flow. Therefore, the equation for the slip-line can be expressed as

$$\frac{\mathrm{d}z}{\mathrm{d}x}=\tan(\varphi-\beta) \tag{10}$$

where φ is the angle between σ_1 and the shear plane, $\varphi=0.5\arccos\left(-n/\left(\sqrt{(\widetilde{\sigma}_x-\widetilde{\sigma}_z)^2+4\tau_{zx}^2}\right)\right)$.

Previous research has demonstrated that listric normal faults and listric reverse faults in gliding fractures resulted from the failures in extending deformation states and compressive deformation states, respectively [9, 13, 35]. Thus, the fracture-line field of the listric reverse fault can be obtained (Fig. 8).

Figure 8 shows that the geometric characteristic of the fracture-line field is a listric type with up-steep and down-gentle, which is supported by actual explorations of F16. The reason for the different angle values is that

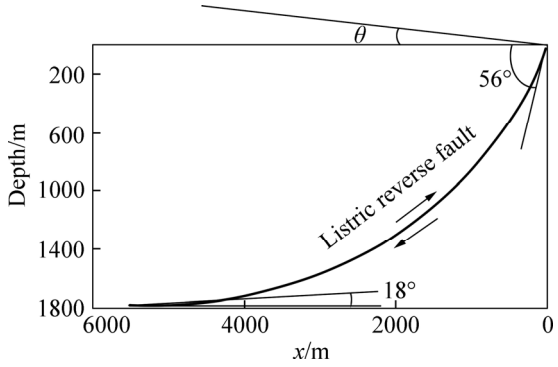

Fig. 8 Fracture-line field of listric reverse fault

the dip angle of the fault calculated in this work (Fig. 8) is the angle between the bedding plane and the fault plane in the beginning of deformation (the bedding plane is (nearly) horizontal). The angle of the field exploration (Fig. 1) contemporarily, however, is the result of late deformation and reformation, which can be confirmed by the existence of the Yima syncline (Fig. 1). The field explorations manifest that the mean dip of the coal seam in the footwall is 12°. Thus, the occurrence of the strata can be returned from its current incline to initial horizontality using the fault's dip angle minus 17° (12°+ θ); therefore, the dip angle values of the fault in its forming stage are obtained: the shallow is 58° and the deep is 0−18°. This result is nearly consistent with the results of the model calculation.

In conclusion, F16 results from the failures in the extending deformation state and its stress state is entirely compressive shear. The geometric characteristics of the fault profile obtained by numerical calculation better reflect the shape of F16 during its initial formation or developmental stage.

6 Mechanical genesis of large-scale reverse thrust sheet

6.1 Stress field of F16

The mechanical model was established by taking a triangular micro-unit from the fault plane as the research area, as shown in Fig. 9.

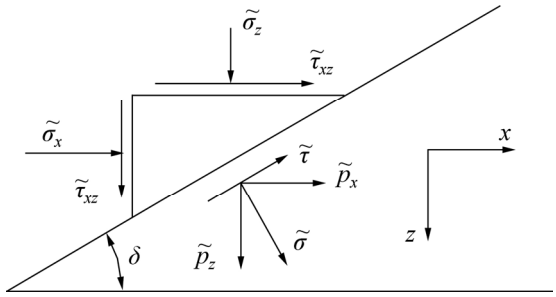

Fig. 9 Mechanical model of thrust fault

The stress components are as follows:

$$\widetilde{\boldsymbol{p}}=\begin{bmatrix}\widetilde{p}_x\\ \widetilde{p}_z\end{bmatrix}=\begin{bmatrix}\widetilde{\sigma}_x & \widetilde{\tau}_{xz}\\ \widetilde{\tau}_{xz} & \widetilde{\sigma}_z\end{bmatrix}\begin{bmatrix}\sin\delta\\ \cos\delta\end{bmatrix}=\begin{bmatrix}\widetilde{\sigma}_x\sin\delta+\widetilde{\tau}_{xz}\cos\delta\\ \widetilde{\sigma}_z\cos\delta+\widetilde{\tau}_{xz}\sin\delta\end{bmatrix} \tag{11}$$

where $\widetilde{p}_x$ and $\widetilde{p}_z$ are the stress components on the fault plane, and δ is the fault's dip angle where the micro-unit is taken.

Further calculations yield the normal stress on the fault plane:

$$\widetilde{\boldsymbol{\sigma}}=\begin{pmatrix}\sin\delta & \cos\delta\end{pmatrix}\begin{bmatrix}\widetilde{p}_x\\ \widetilde{p}_z\end{bmatrix}=\frac{\widetilde{\sigma}_x\tan^2\delta+\widetilde{\sigma}_z+2\widetilde{\tau}_{xz}\tan\delta}{1+\tan^2\delta} \tag{12}$$

The shear stress is as follows:

$$\begin{aligned}\widetilde{\tau}&=\sqrt{\widetilde{\boldsymbol{p}}^2-\widetilde{\boldsymbol{\sigma}}^2}\\&=\left(\widetilde{\tau}_{xz}^2+\frac{\widetilde{\sigma}_x^2\tan^2\delta+\widetilde{\sigma}_z^2+2\widetilde{\tau}_{xz}\tan\delta\left(\widetilde{\sigma}_x+\widetilde{\sigma}_z\right)}{1+\tan^2\delta}-\left(\frac{\widetilde{\sigma}_x\tan^2\delta+\widetilde{\sigma}_z+2\widetilde{\tau}_{xz}\tan\delta}{1+\tan^2\delta}\right)^2\right)^{\frac{1}{2}}\end{aligned} \tag{13}$$

Hence, the stress field of F16 can be obtained based on Eqs. (11), (12), and (13) and Fig. 7, as shown in Fig. 10.

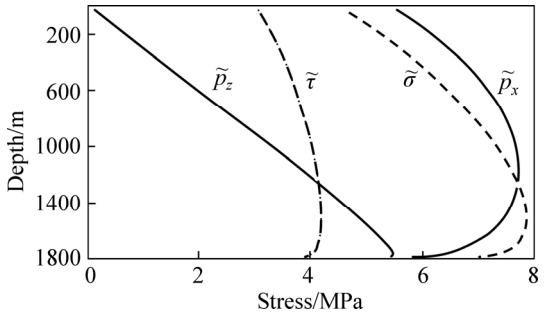

Fig. 10 Stress field of F16

Figure 10 shows that the horizontal stress and normal stress are greater than the vertical stress and shear stress, and both are positive. It also illustrates that F16 is dominated by horizontal stress and its stress state is entirely compressive shear.

6.2 Mechanical mechanisms for slippage of large-scale reverse thrust sheet

The frictional property of the sliding surface is associated with the relative displacement of two fault walls. The initially forming section needs to overcome greater frictional resistance than the existing section to generate relative displacement. With the generation of relative displacement, the surface roughness is subjected to shovels cut and transformations; thus, the frictional resistance decreases.

According to Coulomb's law of friction, there is a positive correlation between frictional stress and the normal stress acting on the fault plane, and the ratio coefficient is called the static friction coefficient. When the shear stress exceeds the static frictional strength, i.e., $\tau>\tau_f$, there will be relative sliding between the hanging wall and the footwall of faults. The static frictional strength can be expressed as

$$\tau_f=\tau_0+\mu\widetilde{\sigma}_f \tag{14}$$

where τ_0 is the strength of anti-friction sliding without normal stress (the cohesion), μ is the friction coefficient, and $\widetilde{\sigma}_f$ is the effective normal stress, τ_0 is generally

considered equal to zero for fault planes; i.e., faults begin to slip when $\tau > \mu\tilde{\sigma}_f$. The friction coefficient decreases once faults start sliding, which is called the dynamic friction coefficient in this case.

The relation between the ratio of shear stress to normal stress ($\tilde{\tau}/\tilde{\sigma}$) and the depth on the fault plane is shown in Fig. 11. BYERLEE [36] found that in the upper crust, the Coulomb friction criterion can be simplified to

$$\begin{cases} \tilde{\tau} = 0.85\tilde{\sigma}; & \tilde{\sigma} < 200\ \text{MPa} \\ \tilde{\tau} = 50 + 0.6\tilde{\sigma}; & \tilde{\sigma} \geq 200\ \text{MPa} \end{cases} \quad (15)$$

As shown in Figs. 10 and 11, $\tilde{\sigma}$ is much less than 200 MPa, and $\tilde{\tau}/\tilde{\sigma}$ is less than 0.85. Hence, in the initial stage of formation of F16, the fault plane is in a state of static friction. Due to the driving friction resulting from the Nanpingquan fault's hanging wall (active plate) thrusting up northward, the strata in the hanging wall of F16 (Nanpingquan fault's footwall) have the trend of clockwise rotation from south to north with the fault plane as the fulcrum (as shown in Fig. 2(b)). At this point, $\tilde{\tau} = \tau_f$ and $\tilde{\sigma} = \sigma_f$, and their relation, which is shown in Fig. 12, can be described as follows:

$$\tilde{\tau} = 0.3371\tilde{\sigma} + 1.534 \quad (16)$$

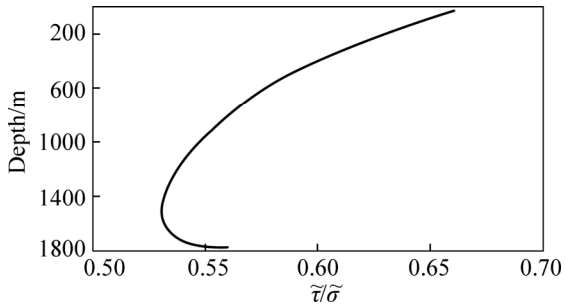

Fig. 11 Relation between $\tilde{\tau}/\tilde{\sigma}$ and depth

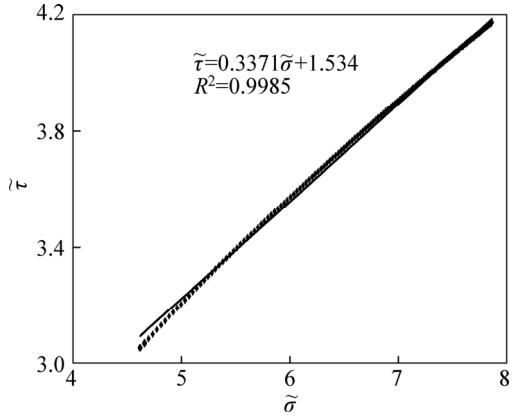

Fig. 12 Relation between shear stress and normal stress in formation stage of F16

With the rotation of strata in the hanging wall of F16, the roughness of the fault plane is subjected to shovel cuts and transformations. The fractured surface forms further, and the frictional resistance decreases. Once the fracture forms, the cohesion τ_0 decreases to zero, and the frictional resistance is transformed from static frictional resistance to dynamic frictional resistance, with values as follows:

$$\tau_f = 0.3371\tilde{\sigma} \quad (17)$$

Consequently, during the sliding period of the strata in the hanging wall of F16, the stress distributed on the north boundary (the active plate of F16) is $\tilde{\tau} - \tau_f$, and stress distributed on of the south boundary (the passive plate of Nanpingquan fault) can be approximated as τ_f (Fig. 12(c)). Figure 13 shows that the values and varieties of τ_f are greater than $\tilde{\tau} - \tau_f$ from top to bottom, resulting in different speeds for the strata in the hanging wall of F16. Eventually, the strata will twist, causing the formation occurrence to steepen and even appear to be upright or inverted (see Figs. 2(c), (d)).

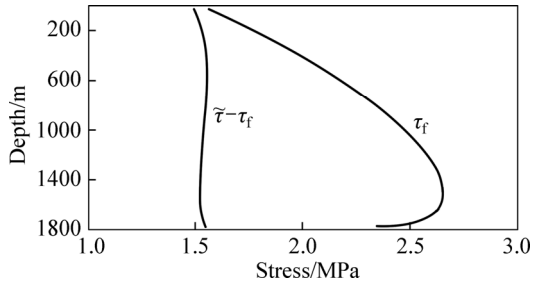

Fig. 13 Stress curves of north and south borders of F16's hanging wall

7 Conclusions

1) A mechanical model of N-S compression superimposed by W-E reverse torsion is established, which satisfactorily explains the tectonic framework of the early Yima coal basin and the formation pattern of Jurassic Yima Group coal measures.

2) The main slip plane (called F16 in the coal mining area) of the Henan Yima thrust nappe structure results from the failures in the extending deformation state and its stress state is entirely compressive shear. The geometric characteristics of the fault profile obtained by numerical calculation can better reflect the shape of F16 in its initial stage of formation.

3) Our model results and the genesis of the large-scale inversion thrust sheet are in some way consistent with the in-situ explorations, which can be significant for further studies on the formation of the thrust nappe structure, the mechanisms of rock bursts induced by F16, and the characteristics of the residual stress field in the Yima mining area.

Acknowledgements

The Institute of Rock Pressure (Henan Dayou Energy Limited Company) and the Yuejin and Qianqiu coal mines provided the data for the local geology. In

particular, we would like to extend a special thanks to Dr. SIGLORY for his useful comments and constructive suggestions, which improved the quality of this paper. We would have never finished this paper so smoothly without the discussions and assistance of Dr. HE Hu and LI Xu-wei.

References

[1] HE Man-chao, QIAN Qi-hu. The basis of deep rock mechanics [M]. Beijing: Science Press, 2010: 310−318. (in Chinese)

[2] HE Jiang, DOU Lin-ming, CAO An-ye, GONG Si-yuan, LV Jian-wei. Rock burst induced by roof breakage and its prevention [J]. Journal of Central South University of Technology, 2012, 19(4): 1086−1091.

[3] CAO Dai-yong, SU Shun-jin. Evolution and occurrence characteristics of Yima coal basin [J]. Coal Geology and Exploration, 1988(6): 11−7. (in Chinese)

[4] CAO Dai-yong, GAO Wen-tai, WANG Chang-xian. The thrust and nappe tectonic zone along the southern margin of the coal-forming region of north China [J]. Journal of China University of Mining and Technology, 1992, 3(1): 103−113.

[5] CHEN Chuan-shi, CAO Yun-xing. The filling and deformation history of Cretaceous and Jurassic on Henan Yima basin [J]. Henan Geology, 1989, 7(3): 37−43. (in Chinese)

[6] CHEN Chuan-shi, CAO Yun-xing. The thrust nappe structure of Henan Yima coalfield [J]. Henan Geology, 1991, 9(3): 31−6. (in Chinese)

[7] YIN X, KOMVOPOULOS K A. Slip-line plasticity analysis of abrasive wear of a smooth and soft surface sliding against a rough (fractal) and hard surface [J]. International Journal of Solids and Structures, 2012, 49(1): 121−31.

[8] ZHAO Lian-heng, YANG Feng. Construction of improved rigid blocks failure mechanism for ultimate bearing capacity calculation based on slip-line field theory [J]. Journal of Central South University, 2013, 20(4): 1047−57.

[9] NYE J F. The flow of glaciers and ice-sheets as a problem in plasticity [J]. Proceedings of the Royal Society of London, 1951, 207(1091): 554−72.

[10] CRANS W, MANDL G, HAREMBOURE J. On the theory of growth faulting: A geomechanical delta model based on gravity sliding [J]. Journal of Petroleum Geology, 1980, 2(3): 265−307.

[11] MANDL G, SHIPPAM G K. Mechanical model of thrust sheet gliding and imbrication [J]. Geological Society, London, special publication, 1981, 9: 79−98.

[12] TAPPONNIER P, MOLNAR P. Slip-line field theory and Large-scale continental tectonics [J]. Nature, 1976, 264: 319−324.

[13] CHEN Qiang. Mechanical research on gravitational structure: Mechanical analysis of listric faults [J]. Seismology and Geology, 1986, 8(3): 11−21. (in Chinese)

[14] MOURGUES R, COBBOLD P R. Sandbox experiments on gravitational spreading and gliding in the presence of fluid overpressures [J]. Journal of Structural Geology, 2006, 28(5): 887−901.

[15] XU Qiang, DONG Xiu-jun. Genetic types of large-scale landslides induced by Wenchuan Earthquake [J]. Earth Science-Journal of China University of Geosciences, 2011, 36(6): 1134−1142. (in Chinese)

[16] MA Run-yong, PENG Jian-bing, MEN Yu-ming, PAN Ai-fang. A study on mechanical mechanism on development of thrust fault [J]. Journal of Northwest University (Natural Science Edition), 2003, 33(2): 196−200. (in Chinese)

[17] DI DOMENICA A, TURTU A, SATOLLI S, CALAMITA F. Relationships between thrusts and normal faults in curved belts: New insight in the inversion tectonics of the Central-Northern Apennines (Italy) [J]. Journal of Structural Geology, 2012, 42: 104−17.

[18] ZHENG Y, ZHANG J, WANG T. Puzzles and the maximum-effective-moment (MEM) criterion in structural geology [J]. Journal of Structural Geology, 2011, 33(9): 1394−1405.

[19] TONG H. Comment and some questions on “puzzles and the maximum effective moment (MEM) criterion in structural geology” [J]. Journal of Structural Geology, 2012, 36(0): 81−84.

[20] LISLE R J, WALKER R J. The estimation of fault slip from map data: The separation-pitch diagram [J]. Tectonophysics, 2013, 583: 158−63.

[21] LI Si-guang. Introduction to geomechanics [M]. Beijing: Science Press, 1979: 125−131. (in Chinese)

[22] WU Zhen-han. New evidence for correlation between global tectonic movement and Earth’s rotation [J]. Journal of Geomechanics, 1995, 1(3): 46−54. (in Chinese)

[23] CHEN Xue-zhong, LI Ye-e, WANG Heng-xin, GUO Xiang-yun. The enhancement of seismicity before the 2004 M_w9.0 Indonesia Sumatra earthquake and its relation to the earth rotation [J]. Chinese Journal of Geophysics, 2013, 56(1): 79−90. (in Chinese)

[24] MA Li-hua, HAN Yan-ben, YIN Zhi-qiang. Progress on variable earth rotation rate and geophysical phenomena [J]. Progress in Geophysics, 2004, 19(4): 968−974. (in Chinese)

[25] MILYUKOV, V K, KRAVCHYUK, V K, MIRONOV, A P, LATYNINA L A. Deformation processes in the lithosphere related to the nonuniformity of the Earth’s rotation [J]. Physics of the Solid Earth, 2011, 47(3): 96−109.

[26] MILYUKOV V, MIRONOV A, KRAVCHYUK V, AMORUSO A, CRESCENTINI L. Global deformations of the Eurasian plate and variations of the Earth rotation rate [J]. Journal of Geodynamics, 2013, 67: 97−105.

[27] ZHAROV V E, GAMBIS D. Atmospheric tides and rotation of the Earth [J]. Journal of Geodesy, 1996, 70: 321−326.

[28] YANG Xue-xiang. The numerical estimation of earth expanding [J]. Crustal Deformation and Earthquake, 1999, 19(4): 80−5. (in Chinese)

[29] OWEN H G. Has the earth increased in size? [C]// New concepts in global tectonics. Lubbock, USA: Texas Technology University Press, 1992: 289−296

[30] GLIKSON A Y. Asteroid/comet impact connections of precambrian episodes: Re-emergence of the catastrophic paradigm in earth science [J]. Earth Science Frontiers (China University of Geosciences, Beijing), 1997, 4(3/4): 23−46. (in Chinese)

[31] WANG Hong-zhen. Speculations on earth’s rhythms and continental dynamics [J]. Earth Science Frontiers (China University of Geosciences, Beijing), 1997, 4(3/4): 1−12. (in Chinese)

[32] WELLS J W. Coral Growth and geochronometry [J]. Nature, 1963, 197(4871): 948−950.

[33] PANNELLA G. Palenotological evidence on the Earth’s rotational history since early Precambrian [J]. Astrophysics and Space Science, 1972, 16(2): 212−237.

[34] CAI Mei-feng, HE Man-chao, LIU Dong-yan. Rock mechanics and engineering [M]. Beijing: Science Press, 2002: 219−226. (in Chinese)

[35] RAMSAY J G. Shear zone geometry: A review [J]. Journal of Structural Geology, 1980, 2(1/2): 83−99.

[36] BYERLEE J D. Friction of rocks [J]. Pure and Applied Geophysics, 1978, 116(4/5): 615−626

(Edited by HE Yun-bin)